AIAA JOURNAL
Vol. 34, No. 5, May 1996

Statistical Saturation of Buoyant Flow Induced by a Fluctuating Acceleration

J. Ross Thomson*
Florida State University, Tallahassee, Florida 32306-4052
and
Jorge Viñals†
Florida A&M University and Florida State University, Tallahassee, Florida 32306

We study buoyancy-driven convection in a laterally heated, two-dimensional cavity under a fluctuating acceleration field, to model flow conditions in a microgravity environment. In the limit of a large aspect ratio cavity (the length in the direction perpendicular to the temperature gradient is much larger than in the parallel direction), an analytic solution can be found in which the flow reaches a statistical steady state of zero average vorticity and mean squared vorticity that scales as the stochastic Rayleigh number squared. We also present the results of a full numerical solution of the Navier–Stokes equation for a fluid driven by a fluctuating acceleration field in a square cavity and confirm the scaling of the flow obtained in the asymptotic analysis.

Nomenclature

d = length in direction of the gradient
G^2 = intensity of fluctuations
R = stochastic Rayleigh number
Ra = Rayleigh number
α = coefficient of thermal expansion of the fluid
ΔT = temperature gradient across the cavity
κ = thermal diffusivity
ν = kinematic viscosity
τ = correlation time

I. Introduction

INTEREST in flow induced by low-amplitude unsteady accelerations is a result of efforts to perform fluid physics or materials processing experiments in a weightless environment. Orbital platforms, such as NASA's Space Shuttle or the proposed space station, serve as the testing ground for many concepts and techniques, which will later serve as a basis for orbital-based manufacturing and other scientific endeavors. These orbital platforms manifest extremely low-amplitude accelerations, known as g jitter, and it is expected that future platforms will as well. In light of this, efforts to measure and analyze the acceleration environment, to understand its acceptable limit parameters, and to develop isolation units are well under way. Multiple origins of the fluctuating acceleration are evident: thruster firing, crew motion, onboard machinery, and atmospheric drag contribute significantly. One perspective is that these forces induce structural vibration modes of the platform, which are then felt at the experiment site. Several effects, such as damping and nonlinear mode coupling, alter the frequency content of the original disturbances. A single vibration frequency may be spread over a wider range, causing a narrow peak in a power spectrum to become broad. Furthermore, the forces ultimately responsible for the disturbances occur at essentially random times and are of random amplitude. Overall, the typical frequency spectrum measured during various Space Shuttle missions is broadband. At low frequencies, typical Fourier amplitudes are $10^{-6}g_E$, increasing to a maximum on the order of $10^{-3}g_E$ at higher frequencies. The effect on experiments of such unsteady residual accelerations is largely an open question.

In this paper we study primarily the effects of a stochastic residual acceleration on buoyancy-induced flow in a laterally heated cavity. In this configuration, flow is induced by the component of the acceleration vector that is perpendicular to the imposed temperature gradient across the cavity. For simplicity, we restrict our analysis to a two-dimensional configuration. This is a good approximation to a three-dimensional flow, if the length of the cavity in the direction perpendicular to the plane defined by the acceleration and gradient directions is sufficiently large. Although our calculations involve idealized conditions and, hence, do not directly simulate a particular materials processing experiment, we expect our results to capture many elements relevant to situations, such as convection in a directional solidification cell, for example.

There has been considerable study of natural convection in the configuration considered here, both analytical and numerical. Some of the earliest workers in this field investigated the scaling behavior of the flow and performed calculations when it was analytically tractable.[1–3] A large number of papers exist that study the flow numerically, to the extent that cavity flow has become a benchmark problem for computational fluid dynamics techniques.[4–9] Flow regimes can be characterized by three independent dimensionless groups: the Rayleigh number Ra, Prandtl number Pr, and the aspect ratio of the cavity A (length of the conducting walls over the length of the adiabatic walls). At sufficiently low values of Rayleigh number, the asymptotic convective flow is time independent (e.g., $Ra < 1.8 \times 10^8$ for $A = 1$ and $Pr = 0.71$). The spatial structure of the steady regime, however, undergoes significant changes as the Rayleigh number is increased, with detailed features of the flow depending on the Prandtl number of the fluid and the aspect ratio of the cavity. The convective flow at the lowest end of Rayleigh numbers is a simple circulation over the entire cavity (for $Ra < 10^3$ in cells of $A = 1$ and $Pr = 0.71$, and for $Ra < 3 \times 10^5$ in $A = 30$ and $Pr = 10^3$). An increase in Rayleigh number results in the formation of boundary layers near the conducting walls. Inside the cavity, large-amplitude stationary waves and recirculating regions near the departing corners of the conducting walls develop for $A = 1$. In the large aspect ratio case, secondary flows leading to a cellular structure are observed at $Ra = 3.6 \times 10^5$. Further increase in Rayleigh number leads to a decrease in the wavelength of the secondary flows, and more cellular regions become visible. Finally, at sufficiently high values of Rayleigh number ($Ra \simeq 1.8 \times 10^8$ for $A = 1$ and $Pr = 0.71$) steady convection undergoes a bifurcation to a time-periodic state.

Received Dec. 20, 1994; revision received May 15, 1995; accepted for publication May 22, 1995.

*Postdoctoral Research Associate, Supercomputer Computations Research Institute.

†Program Director and Associate Professor, Supercomputer Computations Research Institute, Department of Chemical Engineering, College of Engineering.

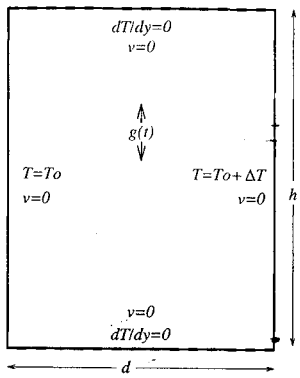

Fig. 1 Configuration of the cavity: vertical walls held at fixed temperature while the top and bottom walls are insulating; velocity taken to be zero on all walls; acceleration forces considered in the vertical direction.

There also exists work considering the effect of an unsteady acceleration on cavity flow.[10–16] In most of these studies, the unsteady acceleration is modeled by a periodic function of time or, alternatively, by a sequence of isolated pulses of short duration. Within the Boussinesq approximation to the Navier–Stokes equation, the coupling between the acceleration field and the density is nonlinear. Thus, it is not clear whether studies in which the acceleration field is approximated by a single or a few periodic components of its frequency spectrum will yield an adequate representation of the actual flowfield in realistic microgravity conditions. Here we adopt what is arguably a more realistic approach, and model the acceleration as a stochastic process in time. We note, however, that even though we model acceleration by a random function that includes a broad distribution of temporal Fourier components, in the parameter range we consider in this paper the density distribution can be well approximated by a linear function of position. Hence, we have not fully addressed the effect of the nonlinear coupling either.

In previous work,[10] we studied the onset of natural convection in a square cavity from a quiescent state, after the acceleration field is turned on. We argued that for a deterministic, single-mode acceleration, the flowfield saturates to a constant amplitude, even in the absence of viscous damping. In the stochastic case, however, and in the absence of viscous damping, the mean squared velocity in the cavity increases linearly with time. Here, we extend our previous work in two directions. First, we consider spatial and temporal degrees of freedom by examining the limit of long aspect ratio cavities. Second, we present a detailed analysis of the flow saturation. The random nature of the acceleration field induces a novel scaling for the (statistically) steady flow. The magnitude of the flowfield is not given by the classical Rayleigh number, but by a modified stochastic Rayleigh number. The flow scaling predicted in the asymptotic analysis is verified for the case of a square cavity by direct numerical solution of the full Navier–Stokes equation.

The configuration studied in this paper is essentially that of standard cavity flow: a Boussinesq fluid is enclosed in a laterally heated, two-dimensional cell of x dimension d and aspect ratio $A = l/d$. The boundary conditions are zero velocity at all of the cavity walls, constant temperature at the two heated walls, and zero normal gradient on the other two walls (see Fig. 1). The initial condition has $v = 0$ everywhere and a uniform temperature gradient across the cavity. At times $t < 0$, the acceleration is zero, and it is turned on at $t = 0$. We only consider in our study an acceleration field perpendicular to the imposed temperature gradient. Although an acceleration parallel to the temperature gradient can induce flow, in the context of the values of the parameters studied in this paper, these effects have been neglected. Indeed, for the component perpendicular to the temperature gradient, there is no finite convection threshold: any acceleration will induce flow and there is no stationary state with zero velocity.

II. Analytic Results

Some general features of the flow that result from the stochastic nature of the acceleration field can be obtained analytically in some limiting cases. First, the limit of long aspect ratio is considered, with flow driven by acceleration fields modeled by either monochromatic or white noises. As discussed further subsequently, individual realizations of monochromatic noise are periodic functions of fixed frequency but random amplitude and phase. This case is akin to more traditional studies in which the acceleration field is modeled by a deterministic periodic function. White noise, on the other hand, has a constant frequency spectrum. The main result of our calculations in this section is that the vorticity at the center of the cavity averages to zero, and its variance is proportional to a stochastic Rayleigh number that we introduce. In Sec. II.B, a more realistic random process for microgravity conditions (narrow-band noise) is introduced. The flow is further simplified in this section in order to study the dependence of the flow on two parameters of the noise: its characteristic frequency and its correlation time.

A. Asymptotic Analysis

We consider, first, analytic solutions of the fluid flow induced by a fluctuating acceleration field, in the limit of a large aspect ratio cavity. When $A \equiv l/d \gg 1$ (see Fig. 2), far enough away from the end boundaries (along the smaller dimension), the velocity and temperature fields are uniform along the y direction. For the case of constant acceleration field, this approximation is essentially exact[17] for Rayleigh numbers $Ra < 10^3$. We then write $\boldsymbol{v} = (u, v) = [0, v(x)]$ and $T = T(x)$. Furthermore, since $(\partial v/\partial y) = 0$, $(\partial T/\partial y) = 0$, and $u(x) = 0$, convective transport of heat and momentum is zero. The temperature now satisfies an equation that is independent of the fluid velocity and, therefore, it will reach a steady state in which the temperature changes linearly across the cavity. With all of these approximations in mind, the Navier–Stokes equation reduces to

$$\frac{\partial v}{\partial t} = \nu \frac{\partial^2 v}{\partial x^2} + \frac{\alpha \Delta T x}{d} g(t) \tag{1}$$

The general solution to this equation with the specified boundary conditions is

$$v(x,t) = -\frac{\alpha \Delta T}{\pi} \sum_{n=1}^{\infty} \frac{(-1)^n}{n} v_n(t) \sin\left(\frac{2n\pi x}{d}\right) \tag{2}$$

where

$$v_n(t) = \int_0^t du g(t-u) \exp\left(-\frac{4\nu}{d^2} n^2 \pi^2 u\right) \tag{3}$$

This is a general result where the form of the acceleration has not yet been specified.

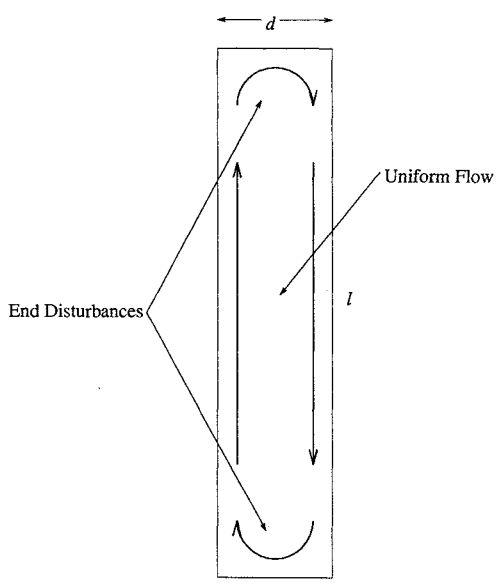

Fig. 2 Long aspect ratio cavity demonstrates uniform asymptotic flow in the region far enough from the ends; flow is steady and uniaxial for $Ra < 10^3$.

1. Deterministic Acceleration

We consider, first, two different types of deterministic acceleration: constant and sinusoidal. For a constant acceleration $g(t) = g_0$, the solution of Eq. (2) is straightforward. We obtain

$$v(x,t) = \frac{\alpha \Delta T g_0 d^2}{4\pi^3 \nu} \sum_{n=1}^{\infty} \frac{(-1)^n}{n^3} \sin \frac{2n\pi x}{d} \times \left[\exp\left(-\frac{4\nu}{d^2} n^2 \pi^2 t \right) - 1 \right] \tag{4}$$

This can be made dimensionless by using the usual variable transformations, $t \to td^2/\kappa$, $v \to vd/(d^2/\kappa)$, and $x \to xd$. The result is

$$v(x,t) = \frac{Ra}{4\pi^3} \sum_{n=1}^{\infty} \frac{(-1)^n}{n^3} \sin 2n\pi x [\exp(-4\pi^2 n^2 Prt) - 1] \tag{5}$$

Here, Rayleigh number and Prandtl number have their usual definitions:

$$Ra = \alpha \Delta T d^3 g_0 / \nu\kappa, \qquad Pr = \nu/\kappa \tag{6}$$

In the limit as $t \to \infty$, the exponential term vanishes leaving a Fourier series for $v(x)$. This series can be summed to give

$$v(x, t \to \infty) = (Ra/6)x\left(x - \tfrac{1}{2}\right)\left(x + \tfrac{1}{2}\right) \tag{7}$$

which is identical to Batchelor's result[1] for the steady-state asymptotic flow in a large aspect ratio cavity. It is important to note here that the scale of the dimensionless velocity is given by the Rayleigh number.

Consider, next, a sinusoidal variation of the acceleration field,

$$g(t) = g_0 \cos(\Omega t + \phi) \tag{8}$$

This case is useful to consider in itself since it leads to two different qualitative limits, depending on whether the response of the fluid is overdamped or underdamped. Substitution of Eq. (8) into Eq. (3) yields $v_n(t)$:

$$v_n(t) = \left\{ g_0 \Big/ \left[\left(\frac{4\nu\pi^2 n^2}{d^2} \right)^2 + \Omega^2 \right] \right\} \times \left\{ \left[\frac{4\nu\pi^2 n^2}{d^2} \cos(\Omega t + \phi) - \Omega \sin(\Omega t + \phi) \right] - \exp\left(\frac{4\nu\pi^2 n^2}{d^2} t \right) \left(\frac{4\nu\pi^2 n^2}{d^2} \cos\phi - \Omega \sin\phi \right) \right\} \tag{9}$$

It is convenient at this point to define a Reynolds number[15] $Re = \Omega d^2/\nu$, also referred to in the literature as the Womersley number.[18] For $t \to \infty$ and after transformation to dimensionless variables, we obtain the expression

$$v(x,t) = \frac{RaPr}{\pi} \sum_{n=1}^{\infty} \frac{(-1)^n}{n} \frac{\sin(2n\pi x)\cos(\Omega t + \phi_n)}{\sqrt{(4Pr\pi^2 n^2)^2 + \Omega^2}} \tag{10}$$

where

$$\phi_n = \phi + \tan^{-1}(\Omega/4Pr\pi^2 n^2) \tag{11}$$

In Eq. (10) each mode v_n has phase lag and amplitude, which depend on n. We can examine two limits of the previous equations: $Re \ll 1$ (overdamped limit) and $Re \gg 1$ (underdamped limit). In the former case, $\phi_n = \phi$ for all n, and the resulting velocity profile is

$$v(x,t) = \frac{Ra}{6} \cos(\Omega t + \phi) x \left(x - \frac{1}{2} \right) \left(x + \frac{1}{2} \right) \tag{12}$$

This is identical to the result in Eq. (7) for a constant acceleration field but modulated by $\cos(\Omega t + \phi)$. In the opposite limit ($Re \gg 1$) $\phi_n = \phi + (\pi/2)$ and the form of the velocity profile is given by

$$v(x,t) = -\frac{Ra}{2\pi\Omega} \cos\left(\Omega t + \phi + \frac{\pi}{2} \right) x \tag{13}$$

In the limit $Re \ll 1$, the viscous boundary layer has penetrated to the saturation limit as determined by the effect of a constant acceleration. That is, the extrema of the velocity profile occur at $x = \pm\sqrt{(1/12)} \simeq 0.289$. The amplitude is not a function of Prandtl number or the angular frequency and is determined by Rayleigh number alone. Furthermore, the velocity field is in phase with the acceleration field. In the opposite limit, $Re \gg 1$, the viscous boundary layer is negligibly thin (of the order of $1/\sqrt{Re}$), the amplitude of oscillation is inversely proportional to Reynolds number, and there is phase lag between the velocity and acceleration fields of $\pi/2$. In both cases, the scale of the dimensionless velocity is set by the value of Rayleigh number.

2. Random Acceleration

In this section, we model g jitter as a stochastic process in time. We consider a particular Gaussian random process, known as narrow-band noise, defined by

$$\langle g(t) \rangle = 0, \qquad \langle g(t) g(t') \rangle = G^2 e^{-|t-t'|/\tau} \cos \Omega(t - t') \tag{14}$$

where the average is taken over an ensemble of realizations of the noise. Ω is a characteristic angular frequency defining the center of the spectral distribution, and τ is the coherence time determining the width of the distribution. This choice is motivated by actual power spectra of the residual acceleration field onboard the Space Shuttle during microgravity missions. From a theoretical point of view, this type of noise permits interpolation between the limit of white noise (in which no frequency component is preferred), and monochromatic noise (similar to a deterministic description). The white noise limit is obtained when $\Omega\tau \to 0$ while $G^2\tau = D$ remains finite, whereas the monochromatic limit is approached as $\Omega\tau \to \infty$ with G^2 finite. In this latter case, the time over which $g(t)$ remains coherent approaches infinity. Typical values of G in microgravity are $G \approx 5 \times 10^{-4} g_E$, where g_E is the intensity of the gravitational field on the Earth's surface, $\tau \approx 1$ s and the angular frequency Ω ranges from 2π s^{-1} to 100π s^{-1}.

Although an explicit solution to Eq. (2) for narrow-band noise can be found, the resulting expression is quite complicated and provides little insight into the effect of the stochastic acceleration on the fluid response. We concentrate first on the limit of white noise and postpone the analysis of narrow-band noise to the next section. Gaussian white noise is obtained from Eq. (14) in the limit of $\Omega\tau \to 0$, with $G^2\tau = D$ finite,

$$\langle g(t) \rangle = 0 \qquad \langle g(t) g(t') \rangle = 2D\delta(t - t') \tag{15}$$

Since the average value of the acceleration vanishes, the average value of the velocity will vanish as well. We calculate the equal time autocorrelation of the velocity, as a function of position by squaring Eq. (2) and taking and ensemble average. We find

$$\langle v^2(x,t) \rangle = \sum_{n=1}^{\infty} \sum_{n'=1}^{\infty} \frac{(-1)^{n+n'}}{nn'} \sin\left(\frac{2n\pi x}{d} \right) \sin\left(\frac{2n'\pi x}{d} \right) v_{nn'}(t) \tag{16}$$

where

$$v_{nn'}(t) = \frac{\alpha^2 \Delta T^2}{\pi^2} \int_0^t du \int_0^t du' \langle g(t-u) g(t-u') \rangle \times \exp\left[-\frac{4\nu\pi^2}{d^2} (n^2 u + n'^2 u') \right] \tag{17}$$

We now substitute Eq. (15) into Eq. (17), and the resulting equation in dimensionless variables is

$$v_{nn'}(t) = \frac{R^2}{4\pi^4} \cdot \frac{1}{(n^2 + n'^2)} \cdot \{1 - \exp[-4Pr\pi^2 (n^2 + n'^2) t]\} \tag{18}$$

where R is the stochastic Rayleigh number defined as

$$R = \alpha \Delta T d^2 \sqrt{2D}/\kappa\sqrt{\nu} \tag{19}$$

and Prandtl number is as defined earlier. For early times and low wave number modes (low n and n'), it is possible to expand the exponential, $1 - e^{-x} \simeq x$, and obtain a closed-form dependence for the early time spatial behavior. The result is

$$\langle v^2(x,t)\rangle = R^2 Pr x^2 t \tag{20}$$

a diffusive growth of the amplitude of the velocity field, in agreement with results presented previously.[10] For late times, the exponential vanishes. In this case, with some manipulation it is possible to sum at least part of the resulting expression. We are left with

$$\langle v^2(x)\rangle = R^2\left\{\frac{x^2}{6}\left(\frac{1}{2}-x\right)\left(\frac{1}{2}+x\right) - \frac{1}{8\pi^3}\sum_{n=1}^{\infty}\frac{(-1)^n}{n^4}\frac{\sinh(2\pi n x)}{\sinh(\pi n)}\sin 2\pi n x\right\} \tag{21}$$

Since the coefficient of $\sin 2\pi n x$ in this equation decreases as $1/n^4$, a sum of the first few terms is adequate to obtain a very reliable numerical estimate of $\langle v^2(x)\rangle$. This function is plotted in Fig. 5.

In summary, under a deterministic forcing, either constant or periodic, the maximum value of the velocity field is proportional to the Rayleigh number. In the stochastic case, however, the mean velocity is zero at all times, and the root mean squared value is proportional to R defined in Eq. (19).

B. Single Mode Description

For more complicated choices of the stochastic acceleration field, the saturation value of the mean squared vorticity depends explicitly on the parameters of the noise. To display this dependence clearly, we consider here the case of narrow-band noise and further simplify the description of the flow. In a sufficiently large cavity, and if the temperature distribution is not significantly affected by the flow, the vorticity in the central region of the cavity will be almost uniform and satisfy

$$\frac{\partial \xi}{\partial t} = -\frac{\nu}{d^2}\xi + \frac{\alpha \Delta T}{d} g(t) \tag{22}$$

This equation can be integrated to obtain

$$\xi(t) = \xi(0)\exp\left(-\frac{\nu}{d^2}t\right) - \frac{\alpha\Delta T}{d}\int_0^t du \exp\left[-\frac{\nu}{d^2}(t-u)\right] g(u) \tag{23}$$

and we choose $\xi(0) = 0$. This corresponds to an initially quiescent fluid, under the influence of zero acceleration.

If $g(t) = g_0$ constant, and in dimensionless variables, $\xi(t) = Ra(1 - e^{-Prt})$. As is well known, the vorticity saturates exponentially in a time scale given by Pr^{-1} to a constant value Rayleigh number. If $g(t) = g_0 \cos(\Omega t + \phi)$ then,

$$\xi(t) = \frac{RaPr}{\sqrt{(Pr)^2 + \Omega^2}}[\cos(\Omega t + \phi') - Pre^{-Prt}] \tag{24}$$

where $\phi' = \phi + \tan^{-1}(\Omega/Pr)$. Once again, we obtain a dimensionless result which includes the usual Rayleigh and Prandtl numbers. In the underdamped limit $Pr \ll \Omega$, the vorticity asymptotically reaches an oscillatory behavior $\xi(t) = RaPr/\Omega \cos[\Omega t + \phi + (\pi/2)]$, consistent with Eq. (12). In the overdamped case, $\xi(t) = Ra \cos(\Omega t)$, consistent with Eq. (13).

We now turn to the case of narrow-band noise and calculate the lowest statistical moments of the vorticity $\langle \xi(t)\rangle$ and $\langle \xi^2(t)\rangle$, where the angle brackets indicate averages over the ensemble. In this paper, the average acceleration is always taken to be zero, which implies that the average vorticity will vanish as well. The second moment is calculated by squaring Eq. (23) and taking an average over the ensemble of acceleration realizations. We obtain

$$\langle \xi^2(t)\rangle = \left(\frac{\alpha\Delta T}{d}\right)^2 \times \int_0^t du \int_0^t du' \exp\left[-\frac{\nu}{d^2}(2t - u - u')\right]\langle g(u)g(u')\rangle \tag{25}$$

where the autocorrelation function of narrow-band noise has been defined in Eq. (14). Integration of Eq. (25) yields

$$\begin{aligned}\langle \xi^2(t)\rangle &= \frac{R^2}{2\tau}\left(\frac{Pr + \tau^{-1}}{(Pr+\tau^{-1})^2 + \Omega^2} - \frac{Pr - \tau^{-1}}{(Pr-\tau^{-1})^2 + \Omega^2}\right) \\ &\times (1 - e^{-2Prt}) + \frac{R^2 Pr \tau^{-1}}{[(Pr-\tau^{-1})^2 + \Omega^2][(Pr-\tau^{-1})^2 + \Omega^2]} \\ &\times \{(Pr^2 + \Omega^2 - \tau^2)(1 + e^{-2Prt}) - 2e^{-(Pr+\tau^{-1})t} \\ &\times [2\Omega\tau^{-1}\sin\Omega t + (Pr^2 + \Omega^2 - \tau^{-2})\cos\Omega t]\}\end{aligned} \tag{26}$$

where we have made the identification $D \equiv G^2\tau$ in the definition of the stochastic Rayleigh number. In the limit as $Pr \to 0$, we recover our previous result[10] involving diffusive growth of the vorticity in the absence of viscous dissipation,

$$\lim_{Pr\to 0}\langle \xi^2(t)\rangle = R^2 Pr\left[\frac{2t}{1+\Omega^2\tau^2} - \frac{\tau}{(1+\Omega^2\tau^2)^2}\{(1-\Omega^2\tau^2) + 2e^{-t/\tau}[2\Omega\tau\sin\Omega t - (1-\Omega^2\tau^2)\cos\Omega t]\}\right] \tag{27}$$

The saturation value of the second moment of the vorticity is now given by

$$\lim_{t\to\infty}\langle \xi^2(t)\rangle = \frac{R^2(Pr\tau + 1)}{2[(Pr\tau+1)^2 + \Omega^2\tau^2]} \tag{28}$$

Finally, in order to clarify the role of the stochastic Rayleigh number, it is illustrative to consider the monochromatic noise limit of Eq. (28), that is, $\tau \to \infty$,

$$\lim_{\tau\to\infty}\lim_{t\to\infty}\langle \xi^2(t)\rangle = \frac{Pr}{2(Pr^2+\Omega^2)}\lim_{\tau\to\infty}\frac{R^2}{\tau} \tag{29}$$

where R diverges as $\sqrt{(\tau)}$. To compare this limit with a fully deterministic description, we define the second moment of a deterministic function $g(t) = g_0 \cos\Omega t$ as

$$\langle g^2\rangle = (1/T)\int_0^T g^2(t)\,dt = g_0^2/2$$

Therefore, in the limit $\tau \to \infty$ $R\sqrt{(Pr)} \to RaPr$, with the identification $g_0^2 = 2G^2$. Thus,

$$\lim_{\tau\to\infty}\lim_{t\to\infty}\langle \xi^2(t)\rangle = \frac{Ra^2Pr^2}{Pr^2+\Omega^2} \tag{30}$$

in agreement with the scaling obtained directly in Eq. (24).

III. Numerical Results

We now turn to the results of a numerical solution of the incompressible Navier–Stokes equation for cavity flow driven by narrow-band noise. We wish to test the scaling predicted by Eq. (28), when no simplifications or assumptions are made regarding the flow. We consider the coupled Navier–Stokes and heat transport equations in the Boussinesq approximation, with boundary conditions appropriate for cavity flow (Fig. 1). The details of the numerical algorithm are given in Ref. 10. Here we summarize the main steps. We use the stream function–vorticity formulation of the Navier–Stokes equation and a forward time-centered space (FTCS) method to solve the time and spatial dependence. Successive overrelaxation (SOR)

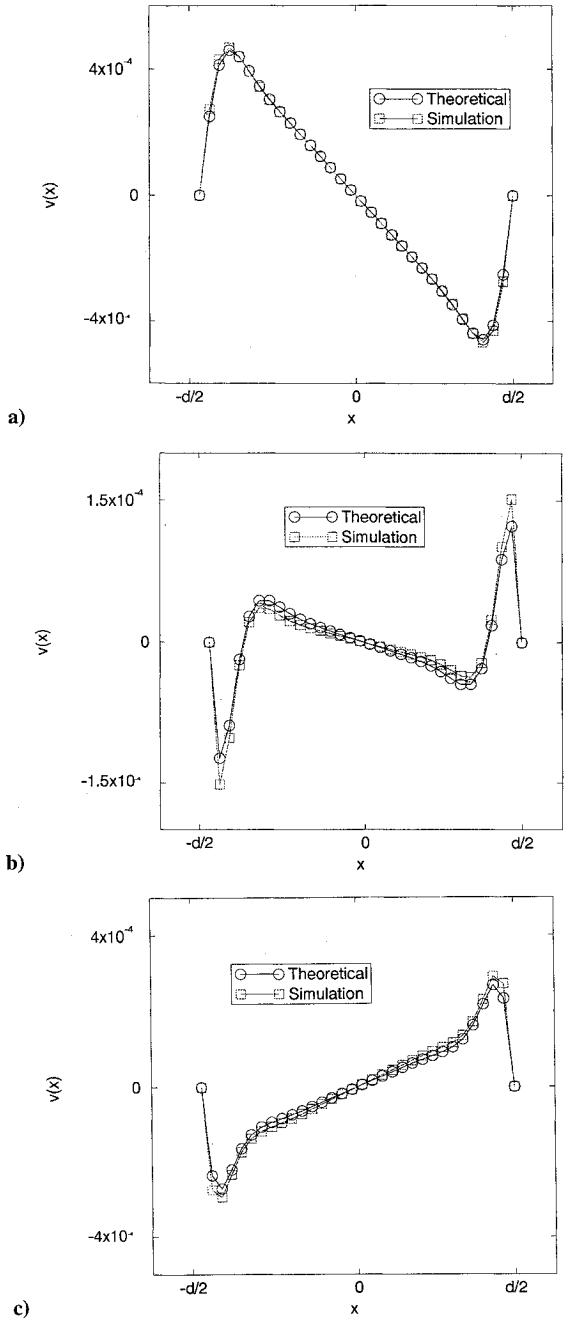

Fig. 3 Velocity profile at the midpoint of a long aspect ratio cavity for flow induced by a sinusoidal acceleration; $Ra = 1, Pr = 700, \Omega = 1.4 \times 10^4$: a) time at which the maximum value of v is reached and b) and c) two intermediate times.

is used to solve the Poisson equation relating the stream function and vorticity. The stochastic terms are integrated separately by using a first-order integration scheme described in detail in Refs. 10 and 19. All solutions were obtained on a spatially uniform grid. For the long aspect ratio ($A = 8$), we employed a 32×256 node grid, whereas for $A = 1$ we consider 32×32 nodes. In the case of a stochastic acceleration, and for each set of conditions, the results have to be averaged over an ensemble of independent realizations of the noise. All of the results that we show subsequently for $A = 1$ correspond to averages over 50 independent realizations. For the case $A = 8$ driven by white noise, we have considered a single realization and, instead, averaged the square of the velocity over 20,000 time steps once the flow has reached saturation.

A. Long Aspect Ratio Cavity

We have first studied the flow in a large aspect ratio cavity to validate the accuracy of the numerical algorithm. At the lower end of the range of Reynolds numbers considered, the velocity field

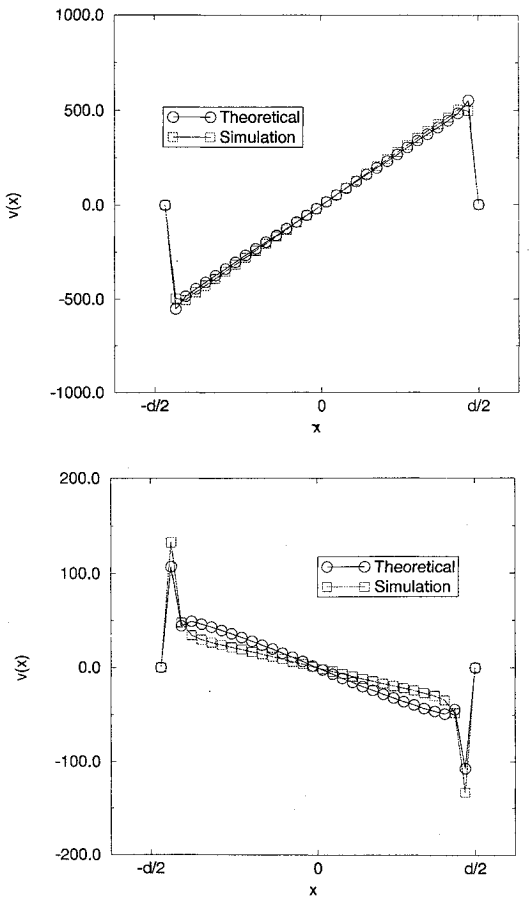

Fig. 4 Velocity profile at the midpoint of a long aspect ratio cavity for flow induced by a sinusoidal acceleration; $Ra = 10^5$, $Pr = 70$, $\Omega = 1.4 \times 10^5$; profile is nearly that of the sawtooth form predicted: a) time at which the maximum value of v is reached and b) intermediate time.

changes smoothly across the cavity. At larger Reynolds numbers, a thin boundary layer of width $1/\sqrt{(Re)}$ develops at the walls that needs to be resolved in order to properly account for the contribution from viscous dissipation to saturation. The numerical difficulty is somewhat alleviated by the fact that the velocity field averages to zero, and its mean squared value decreases as $1/Re$ for large Reynolds number. We have checked that the algorithm reproduces the asymptotic solution for a deterministic, sinusoidal acceleration, both at low nd relatively high Reynolds number, and for white noise. In this latter case, there is a very broad spectrum of frequency components that contribute to the flow.

First we examine the limit of moderate Reynolds number. In Figs. 3a–3c, the analytical and numerical solutions are compared for three particular times. This example is of extremely low Rayleigh number and relatively large Prandtl number with a dimensionless angular frequency of 1.4×10^4. Figure 3a shows the time at which the maximum velocity is attained, whereas Figs. 3b and 3c show other intermediate times. One interesting features of these profiles is the observation that the boundary-layer flow actually precedes in phase the flow in the bulk.

Figures 4a and 4b show profiles for a different set of parameters ($Ra = 10^5$, $Pr = 70$ and $\Omega = 1.4 \times 10^5$) chosen so that the velocity profile is that of a sawtooth, as was predicted for large forcing frequencies. The numerical solution also agrees with the asymptotic analysis. We note, however, that since the Reynolds number is quite high, the acceleration induces a flow several orders of magnitude less than one would expect for the large Rayleigh number used. This can also be seen from the scaling of Eq. (12).

We next turn to a stochastic forcing, and consider the case of white noise in the large aspect ratio limit. Figure 5 shows the second moment of the velocity in the cavity, $\langle v^2 \rangle / R^2$. As discussed, the average has been computed over a sample of 20,000 time steps once the velocity field has reached saturation in a statistical sense. Again,

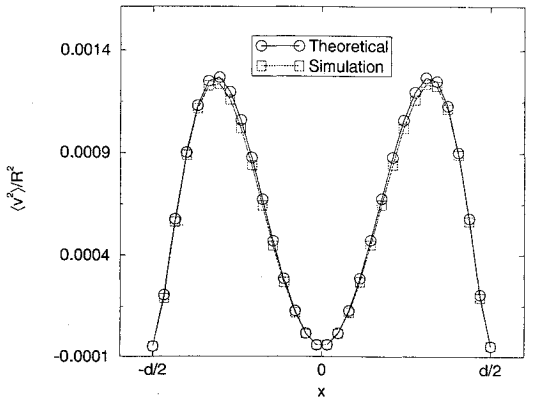

Fig. 5 Second moment of the velocity normalized by R^2 as a function of position in the cavity in the limit of long times.

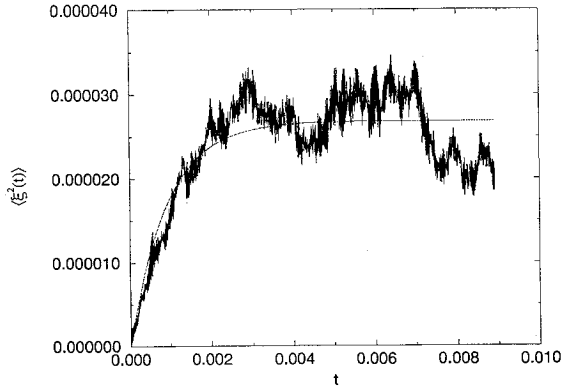

Fig. 6 Simple exponential fit to $\langle \xi^2(t) \rangle$; $R = 2.30$, $\Omega\tau = 62.5$; Fig. 7 plots saturation values obtained with this method.

the numerical simulation is in good agreement with the asymptotic analysis.

B. Square Cavity

Finally, we have studied numerically the saturation of the flow in a square cavity under the influence of narrow-band noise. The range of parameters of the fluid and of the noise considered have been chosen to represent typical fluids and microgravity conditions, while being consistent with the condition that the temperature field is not appreciably distorted by the flow. In this limit we are interested primarily in the mechanical response of the fluid to a random acceleration with small or negligible convective transport. It is only in this limit that we have been able to obtain some analytic understanding of stochastic effects on the flow. We do plan, however, to extend our analysis to other more complex cases in the future. For each of the parameter values to be described, 50 flow simulations with independent realizations of narrow-band noise were averaged.

Our results were analyzed in terms of both the vorticity and the stream function at the center of the cavity. Both exhibit similar trends, and we show here only the values of the vorticity. In Fig. 6 we illustrate the fitting procedure used to obtain the saturation value of the vorticity at the center of the cavity: the time dependence approximated by an exponential function. The time constant of the exponential scales linearly with the Prandtl number, as expected. The saturation values, for a wide range of Prandtl numbers and of fluid parameters, are shown in Fig. 7 as a function of R^2. This figure demonstrates the linear dependence of the $\langle \xi^2(t) \rangle$ saturation value with R^2, as predicted in Eq. (28), for a wide range of values of R.

IV. Summary

The analysis of cavity flow in a long aspect ratio clearly describes the flow with some accuracy, if the rate of flow is less than that which induces the "cat-eye" instability described by Elder.[17] The agreement between the numerical solutions of the full Navier–Stokes equations and the analytic solution verifies that the grid size used

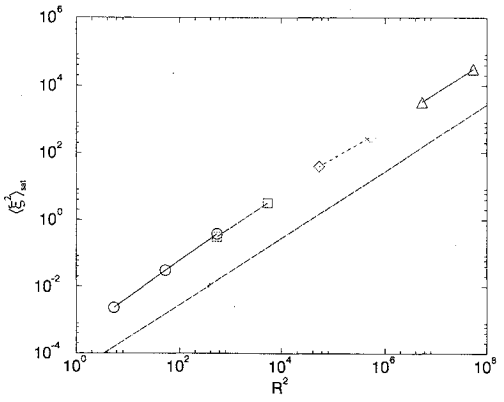

Fig. 7 Dependence of $\langle \xi^2_{sat} \rangle$ on R; each point corresponds to an average over 50 independent runs, for fixed $\tau = 1.4 \times 10^{-5}$ and $Pr = 7.1 \rightarrow 710$; as predicted in Eq. (28), the scaling of the saturation vorticity is given by R^2; $\Omega\tau = 6.25$.

in our solutions is adequate to capture most of the details of the flow. Even at large Reynolds number, since the flow velocity scales like Ra/Re in the deterministic case, the grid that we have used is enough to resolve the boundary layer at the walls.

The qualitative behavior of the flow under a sinusoidal acceleration in the long aspect ratio limit is quite interesting. Since the evolution of each spatial mode is independent in this limit, the effect of the phase differences between the modes becomes evident: for very low frequencies ($Re \ll 1$) and very high frequencies ($Re \gg 1$) all spatial modes remain in phase, and time variation is essentially one of amplitude. These two situations are distinct, however, since for the low frequency, all modes are in phase with acceleration, whereas for the high frequency, there is a phase lag of $\pi/2$. In the transition from one extreme to the other, modes of different spatial frequency develop phase relationships depending on the angular frequency Ω of the acceleration and on the wave number n of the spatial mode. The most interesting result of this is that at some points in the period of oscillation, the flow along the boundary layer actually precedes the flow in the center of the cavity, giving rise to the interesting velocity profiles seen in Figs. 3b and 3c.

For a deterministic acceleration, the flow will reach a steady state, be it constant flow as obtained for constant acceleration, or oscillatory flow as obtained for a sinusoidal acceleration, in times which scale like the Prandtl number. The magnitude of the flow velocity scales with the Rayleigh number Ra. For the stochastic case, however, the time required to reach saturation is still proportional to the Prandtl number, but the saturation velocity averages to zero and has a standard deviation around this mean proportional to the stochastic Rayleigh number defined in Eq. (19). This scaling has been confirmed numerically in the case of a square cavity and is depicted in Fig. 7.

We expect that our results describe many of the qualitative features of g-jitter induced convection in more realistic situations. For example, Eq. (24) captures the main features of the flow obtained in the numerical calculations of Alexander et al.,[13] who studied the onset of natural convection in cells appropriate for crystal growth by the Bridgman–Stockbarger method. In this latter case, of course, there is coupled transport of mass and heat, and more complicated boundary conditions both at the walls of the cavity and at the crystal-melt interface. At large values of $Re \approx 5000$, the maximum fluid velocity predicted by Eq. (24) agrees with the simulations. They further observed a phase difference of $\pi/2$ between $g(t)$ and $\xi(t)$, as predicted. As expected, our predictions become less accurate for smaller values of Reynolds number. At $Re \approx 5$, our prediction for the maximum flow velocity overestimates the simulation by a factor of 2, although we agree with the simulations in that $g(t)$ and $\xi(t)$ are almost in phase.

We finally note that the scaling predicted in this work applies to the regime in which there is no appreciable convective transport, either for large aspect ratio cavities or when $\Omega/Pr = 1/Re \ll 1$. The reason why this limit has been addressed first is that the simplicity of the flow has allowed us a fairly complete analytic study. The main focus of the study has been on the mechanical response of

a fluid subject to a fluctuating acceleration, setting aside further complications due to transport.

Acknowledgments

This work is supported by the Microgravity Science and Applications Division of NASA under Contract NAG3-1284. This work is also supported in part by the Supercomputer Computations Research Institute, which is partially funded by the U.S. Department of Energy, Contract DE-FC05-85ER25000. We thank Jaume Casademunt for his important contributions in the early stages of this work.

References

[1]Batchelor, G. K., "Heat Transfer by Free Convection Across a Closed Cavity Between Vertical Boundaries at Different Temperatures," *Quarterly of Applied Mathematics*, Vol. 12, 1954, p. 209.

[2]Gill, A. E., "The Boundary–layer Regime for Convection in a Rectangular Cavity," *Journal of Fluid Mechanics*, Vol. 26, 1966, p. 515.

[3]Patterson, J., and Imberger, J., "Unsteady Natural Convection in a Rectangular Cavity," *Journal of Fluid Mechanics*, Vol. 100, 1980, p. 65.

[4]Davis, G. D. V., "Natural Convection of Air in a Square Cavity: A Bench Mark Numerical Solution," *International Journal for Numerical Methods in Fluids*, Vol. 3, 1983, p. 249.

[5]Quere, P. L., and Roquefort, T. A. D., "Computation of Natural Convection in Two-Dimensional Cavities with Chebyschev Polynomials," *Journal of Computational Physics*, Vol. 57, 1985, p. 210.

[6]Wang, T.-M., and Korpela, S. A., "Convection Rolls in a Shallow Cavity Heated from a Side," *Physics of Fluids A*, Vol. 6, 1989, p. 947.

[7]Kuo, H. P., and Korpela, S. A., "Stability and Finite Amplitude Natural Convection in a Shallow Cavity with Insulated Top and Bottom and Heated from a Side," *Physics of Fluids*, Vol. 31, 1988, p. 23.

[8]Ramaswamy, B., Jue, T. C., and Akin, J. E., "Finite Element Analysis of Oscillatory Flow with Heat Transfer Inside a Square Cavity," *AIAA Journal*, Vol. 30, 1992, p. 412.

[9]Wilkes, J. O., and Churchill, S. W., "The Finite-Difference Calculation of Natural Convection in a Rectangular Enclosure," *AIChE Journal*, Vol. 12, 1966, p. 161.

[10]Thomson, J. R., Casademunt, J., and Viñals, J., "Cavity Flow Induced by a Fluctuating Acceleration Field," *Physics of Fluids*, Vol. 7, 1995, p. 292.

[11]Jue, T. C., and Ramaswamy, B., "Natural Convection with Thermocapillary and Gravity Modulation Effects in Low-Gravity Environments," *Journal of Spacecraft and Rockets*, Vol. 29, 1992, p. 856.

[12]Alexander, J. I. D., "Low-gravity Experiment Sensitivity to Residual Acceleration: a Review," *Microgravity Science and Technology*, Vol. 3, 1990, p. 52.

[13]Alexander, J. I. D., Amiroudine, S., Ouazzani, J., and Rosenberger, F., "Analysis of the Low Gravity Tolerance of Bridgman–Stockbarger Crystal Growth II. Transient and Periodic Accelerations," *Journal of Crystal Growth*, Vol. 113, 1991, p. 21.

[14]Biringen, S., and Danabasoglu, G., "Computation of Convective Flow with Gravity Modulation in Rectangular Cavities," *Journal of Thermophysics and Heat Transfer*, Vol. 4, 1990, p. 357.

[15]Kamotani, Y., Prasad, A., and Ostrach, S., "Thermal Convection in an Enclosure Due to Vibrations Aboard a Spacecraft," *AIAA Journal*, Vol. 19, 1981, p. 511.

[16]Farooq, A., and Homsy, G. M., "Streaming Flows due to g-Jitter-induced Natural Convection," *Journal of Fluid Mechanics*, Vol. 271, 1994, p. 351.

[17]Elder, J., "Laminar Free Convection in a Vertical Slot," *Journal of Fluid Mechanics*, Vol. 23, 1965, p. 77

[18]Kurzweg, U. H., "Enhanced Heat Conduction in Oscillating Viscous Flow Within Parallel-plate Channels," *Journal of Fluid Mechanics*, Vol. 156, 1985, p. 291.

[19]Zhang, W., Casademunt, J., and Viñals, J., "Study of the Parametric Oscillator Driven by Narrow Band Noise to Model the Response of a Fluid Surface to Time-dependent Accelerations," *Physics of Fluids A*, Vol. 5, 1993, p. 3147.